Parametric Study of a 1.5-D Combustion Chamber Model on the Hybrid Rocket Engine Performances

Elena Quero Granado, Jouke Hijlkema, Jean-Yves Lestrade, Jérôme Anthoine

DOI: 10.13009/EUCASS2022-5651
9TH EUROPEAN CONFERENCE FOR AERONAUTICS AND SPACE SCIENCES (EUCASS)

Parametric Study of a 1.5-D Combustion Chamber Model on the Hybrid Rocket Engine Performances

Elena Quero Granado⋆†*, Jouke Hijlkema*⋆*, Jean-Yves Lestrade*⋆ *and Jérôme Anthoine*⋆
⋆*ONERA / DMPE, Université de Toulouse*
F-31055 Toulouse, France
elena.quero_granado@onera.fr · jouke.hijlkema@onera.fr · jean-yves.lestrade@onera.fr · jerome.anthoine@onera.fr
†Corresponding author

Abstract

A sensitivity analysis of a 1.5-D combustion chamber model of a hybrid rocket engine is performed in this paper. The goal is to assess the impact that some of the most important engine parameters have over its performances. Studies are carried out by considering three categories of parameters: the aerodynamic characteristics at the inlet of the chamber, the thermochemical quantities involved in the gas-surface interaction model, and the geometrical properties of the fuel block. Simulations have been made at steady-state regime for a cylindrical, lab-scale combustion chamber with a 1-D nozzle model, using mainly gaseous oxygen as oxidizer and high density polyethylene as fuel. The fundamental reference variables used for the sensitivity studies have been the regression rate, the averaged chamber pressure, the radial profiles of temperature and species mass fractions, and the thrust and specific impulse of the engine. Fuel regression rate results have shown a high dependence upon the oxidizer mass flux, the motor size, the number of ports of the fuel block, and the variables intervening directly on the energy balance at the fuel surface, such as the radiative heat flux source and the composition of the solid fuel. The retrieved influence of these parameters on engine performances has been found to be in agreement with the literature data, being in some cases of the same intensity.

Nomenclature

Letters

$\Delta H^0_{f,k}$	Specific enthalpy of formation of the species k, J/kg
ΔH_{pyr}	Specific enthalpy of pyrolysis of the fuel, J/kg
δ	Boundary layer thickness, m
δ^*	Displacement thickness, m
$\dot{\omega}_k$	Production rate of species k at the fuel surface, kg/m^2/s
$\dot{Q}_{rad}$	Net radiation heat flux, W/m^2.
η	Radial coordinate, reference at the fuel surface
η_c	Combustion efficiency
γ	Heat capacity ratio
$\mathcal{M}_k$	Molar mass of the species k, kg/mol
ρ	Density, kg/m^3
τ	Viscous stress term, N/m^2
θ	Momentum thickness, m
A_d	Arrhenius preexponential constant, m/s
$a_{thermal}$	Thermal diffusivity, m^2/s
B	Blowing number
C_f	Skin friction coefficient
c_F	Theoretical thrust coefficient on the ground
c_p	Specific heat constant, J/kg/K
D	Diameter of the fuel port, m
D_{diff}	Diffusion coefficient, m^2/s
E_a	Activation energy in the Arrhenius pyrolysis law, J/mol
F	Thrust force generated by the engine, N
G	Fuel mass flux, kg/m^2/s
h_D	Mass diffusion coefficient, m/s
h_t	Specific total enthalpy, J/kg
h_{conv}	Heat convection coefficient, W/m^2/K
k	Thermal conductivity, W/m/K
L	Length of the fuel block, m
N_{sp}	Total number of species in the gas flow
P	Pressure, Pa
R	Radius of the fuel port, m

DOI: 10.13009/EUCASS2022-5651

r	Radial coordinate, reference to the chamber axis
R_g	Gas constant, J/kg/mol
S	Cross sectional area, m^2
Sc	Schmidt number
St	Stanton number
T	Temperature, K
t	Time, s
u	Axial velocity component, m/s
v	Radial velocity component, m/s
x	Axial coordinate
Y_k	Mass fraction of the species k

Subindex

amb	Evaluated at ambient conditions
ch	Averaged values at the chamber
e	Core flow region
f	Corresponding to the solid fuel
hyb	Corresponding to the hybrid phase of the engine
in	Inlet conditions at the combustion chamber
out	Conditions at the exit of the nozzle
ox	Oxidizer conditions at the chamber entrance
pyr	Corresponding to fuel pyrolysis
r	Fuel regression
ref	Reference value
s	Evaluated at the fuel surface
th	Evaluated at the nozzle throat

1. Introduction

In recent years, Hybrid Rocket Engines (HREs) have become, increasingly attractive as an alternative to conventional chemical propulsion systems because of their throttleability capability, reduced production cost, and higher safety and performance in comparison with their rocket propulsion counterparts (liquid and solid). These advantages allow their application for sounding rockets, small satellite launchers or even orbital propulsion systems. This technology is characterized by the combustion of two propellants stored at different states of the matter: generally, the oxidizer, stored in the liquid or gaseous state, is introduced into the combustion chamber, where the combustible is in the solid state. The high temperatures attained by the injection of a hot gaseous oxidizer or by the use of a pyrotechnic device at the start of the engine operation, pyrolyzes the solid fuel, whose products react with the oxidizer, originating a turbulent diffusion flame inside the boundary layer (BL) situated at a certain distance above the fuel surface. Finally, the gas products resulting from combustion are expelled through the nozzle, generating thus, the thrust of the engine.

The conception of a HRE requires the knowledge of the engine performances in a large number of configurations / conditions that will allow the optimization of its design to accomplish a specific mission (required ΔV and/or total spacecraft mass) whilst enhancing some engine characteristics such as the payload mass, the thrust level, the nozzle expansion ratio, etc.. Several authors[12,16,29] have already developed tools for the design of HREs. However, these applications implement 0-D or 1-D models to describe the pyrolysis process of the fuel inside the combustion chamber through semiempirical laws[21] that are dependent on the geometrical and dimensional characteristics of the engine, as well as the Oxidizer / Fuel (O/F) couple used in the experimental tests performed to obtain them, not allowing a general application thereof for a HRE system system design tool, since it is required to have already performed the experimental tests at the conditions that want to be simulated. Otherwise, RANS 2-D simulations of the combustion chamber provide high precision regression rate values (lower than 15%)[3,7,26] when taking into account a more detailed chemistry, the flow turbulence and the radiation phenomena in the combustion chamber. Nevertheless, the large computing time thereof represents a substantial hindrance for their use during the engine pre-design phases. With the purpose of merging both aspects of higher accuracy and reduced computational cost to better fit the requirements of the design tools employed during these phases, an approximate 2-D modeling (also known as 1.5-D model), based on the integral BL methods and reproducing the most important physics inside the combustion chamber has been developed. This kind of models has been used in literature before to simulate non-reactive and reactive flows.[2,20] They have proven to be less time-consuming in comparison to a full Navier-Stokes solver while supplying satisfactory results. A 30% deviation between the experimental and the numerical results can be accepted in our model in order to make it competitive for the envisaged system design tool face to the other existing design applications.

In this paper, a brief presentation of the aforementioned model has been made. The first validation phase of this one was carried out in Quero Granado et al.'s work,[13] where the computed results for the non-reactive and the reactive flow cases were compared to data from literature and with three experimental tests performed on the HYCAT (Hybrid with Catalyst) hybrid engine of our laboratory. However, the numerical simulations were performed for some specific properties / characteristics of the flow and the solid fuel, whose overestimation or underestimation may have induced significant changes in the ablation physics, impacting thus the computed results and increasing or diminishing the discrepancies with the references. The characterization of the fuel regression rate (key variable in the estimation of

DOI: 10.13009/EUCASS2022-5651

HRE thrust) depends on a large number of parameters related to the flow. Indeed, the combustion process is strongly coupled to the degradation of fuel and the aero-thermo-chemical phenomena of the flow. The effect of the choice of some modeling parameters on the predictions of the HRE performances requires to be quantified because there can be uncertainties or inaccuracies on their estimate values. Actually, values of some of the properties describing the fuel or the pyrolysis process are found to be widely scattered in literature. Several authors have already analyzed the impact of some of these features.[3,4,6,17] Hence, this paper has focused on the realization of a sensitivity analysis to determine the most adequate modeling and highlight the key parameters influencing the calculation of the HRE performances.

2. Presentation of the 1.5-D Combustion Chamber Model

The 1.5-D model presented in this paper comes from an aproximation of the two-dimensional equations of the flow: it is based on the integration of the fluid dynamics equations along the radial direction of the chamber followed by the numerical calculation of the resulting equations along of the motor axis.
The flow in the combustion chamber is considered to be axially injected at the gaseous state. Knowing that transition from a laminar to a turbulent flow (between $2300 < Re < 10^4$ for a non-reactive flow in a circular duct) happens at smaller Reynolds numbers when the boundary layer is exposed to evaporation phenomena or blowing from the fuel surface, the flow inside the chamber of a hyrbid rocket ($Re = \rho u D/\mu > 10^4$), is considered to be fully turbulent. In addition, Prandtl (Pr) and Lewis (Le) numbers are taken equal to unity for the sake of simplicity, implying also that the molecular diffusion coefficient (D_{diff}) is the same for all the species in the flow. The transient, compressible and reactive form of the fluid mechanics equations is employed to describe the flow in the combustion chamber. This one follows two configurations: a developing flow and a fully developed one. In the first case, the flow is divided in two areas along the radial dimension: an inviscid zone representing the core flow; and the region of the boundary layer where the flame is located. This one is represented by an infinitely fast, irreversible chemistry, happening at stoichiometric conditions, whose temperature is computed by CEA thermochemical equilibrium code through a constant temperature-pressure problem. Moreover, for simplification, combustion is described by a single global reaction, where only the species CO_2 and H_2O are considered as products. Figure 1 depicts the graphical representation of this model.

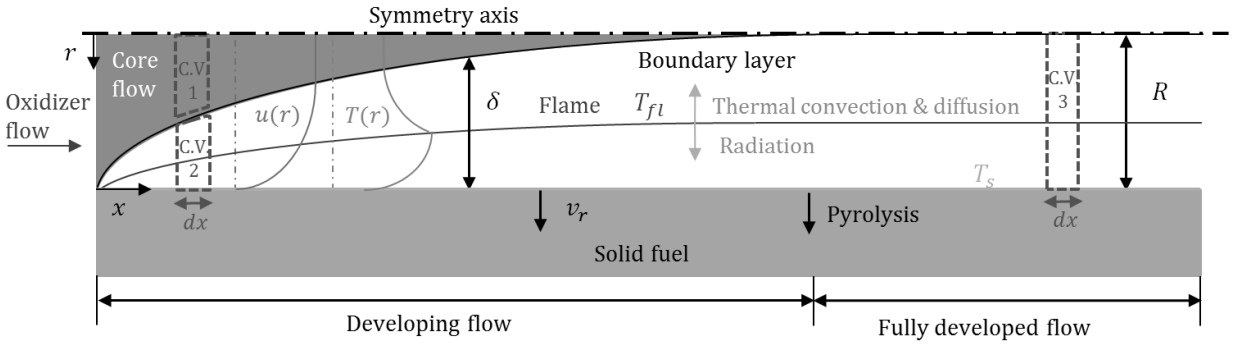

Figure 1: Representation of the flow and the involved physical phenomena inside the combustion chamber of a HRE for the model presented in this paper

Proceeding with the radial integration of the axisymmetric-coordinates equations describing the core and viscous flow regions and by employing the Leibnitz integral rule, the core flow (Euler) equations ($0 \leq r \leq R - \delta$) are defined by the continuity, quantity of momentum and species mass fraction balances [Eqs. (1) to (4)]. Here, an ideal gas law is considered and described by the flow state equation [Eq. (5)]. Whilst using the same procedure, the boundary layer region ($R - \delta \leq r \leq R$) is defined by the continuity [Eq. (6)] and axial quantity of momentum [Eq.(7)] balances. More details about the model and the procedure to attain these expressions can be found in Quero Granado et al.[13] The fully developed flow configuration equations can be deduced easily by integrating the previous equations along the whole radius of the channel and will not be thus showed in this paper.

$$\rho_e \frac{du_e}{dt} + \rho_e u_e \frac{du_e}{dx} = -\frac{dP}{dx} \tag{1}$$

$$\frac{dP}{dr} = 0 \tag{2}$$

$$\rho_e \frac{dh_{t,e}}{dt} + \rho_e u_e \frac{dh_{t,e}}{dx} = \frac{dP}{dt} \tag{3}$$

DOI: 10.13009/EUCASS2022-5651

$$\begin{cases} \rho_e \frac{dY_{k,e}}{dt} + \rho_e u_e \frac{dY_{k,e}}{dx} = 0 \quad \text{for } k = 1, 2...N_{sp} - 1 \\ \sum_{k=0}^{N_{sp}} Y_{k,e} = 1 \end{cases} \tag{4}$$

$$P_e = \rho_e \left(\sum_k^{N_{sp}} Y_{k,e} \frac{R_g}{\mathcal{M}_k} \right) T_e \tag{5}$$

$$\frac{d}{dt}\left\{ \frac{1}{2}\left[R^2 - (R-\delta)^2 \right] \bar{\rho} \right\} + \frac{d}{dt}\left[\frac{1}{2}(R-\delta)^2 \rho_e \right] + \frac{d}{dx}\left[\frac{1}{2}(R-\delta^*)^2 \rho_e u_e \right] - \rho_s v_s R = 0 \tag{6}$$

$$\begin{aligned} &\frac{1}{2}(R-\delta^*)^2 u_e \frac{d\rho_e}{dt} + \frac{1}{2}\left[(R-\delta^*)^2 - (R-\delta)^2 \right] \rho_e \frac{du_e}{dt} + \rho_e u_e (R-\delta^*) \frac{d(R-\delta^*)}{dt} + \rho_e u_e^2 \left[R - (\delta^* + \theta) \right] \frac{d\left[R - (\delta^* + \theta) \right]}{dx} \\ &+ \frac{1}{2}\left[R - (\delta^* + \theta) \right]^2 u_e^2 \frac{d\rho_e}{dx} + \rho_e u_e \frac{du_e}{dx} \left\{ \left[R - (\delta^* + \theta) \right]^2 - \frac{1}{2}(R-\delta)^2 \right\} = -\frac{dP}{dx} \frac{1}{2}\left[R^2 - (R-\delta)^2 \right] - \tau_{xy,s} R \end{aligned} \tag{7}$$

The integration of the equations in the radial direction requires the introduction of closure models. Empirical profiles describing the radial variation of the main quantities in the BL, such as the axial velocity, the species mass fractions, and the temperature are thus, employed. The velocity distribution used is given by Eq. (8)[23] with $n = 1/7$, where the acceleration at the flame zone has been neglected. Additionally, the Reynolds analogy allows to relate the mass and heat transfers, establishing then an equivalence between the total entalpy and the species mass fractions through the Shvab-Zeldovich scalar variable ($z = Y_F - Y_O / r_M$) profiles.

$$\frac{u}{u_e} = \left(\frac{\eta}{\delta} \right)^n = \frac{h_t - h_{t,s}}{h_{t,e} - h_{t,s}} = \frac{z - z_s}{z_e - z_s} \tag{8}$$

Besides, the viscous stress term from Eq. (7) is defined by a wall friction coefficient that is modified by the fuel blowing effect at the wall[1] through $B = \frac{\rho_f v_r}{\frac{1}{2} C_f \rho_e u_e}$ [see Eq. (9)]. In this equation, C_{f0} is the local skin friction coefficient when no mass is injected through the wall, given by Eq. (10), and $C_{f0,D}$ is the coefficient in the developed flow region, which is defined by Bhatti and Shah's expression for a circular duct.[23]

$$\frac{C_f}{C_{f0}} = \begin{cases} B^{-0.68} & \text{for } 5 < B < 20 \\ \frac{1}{1+0.4B} & \text{for } B \leq 5 \end{cases} \tag{9}$$

$$\frac{C_{f0}(x)}{C_{f0,D}} = 1 + C_1 Re_D^{-\alpha} \exp(-\beta x / D) \tag{10}$$

Finally, in order to close the system of equations, the boundary conditions at the fuel surface are applied through the Gas-Surface Interaction (GSI) model, which is based on the realization of different balances between the gas and the solid fuel in a quasi-steady state. Here, it is established that the mass lost during the fuel degradation by pyrolysis is entirely transmitted to the flow [see Eq. (11)]. Moreover, in the mass species balance, the gaseous fuel has been considered as the only species resulting from pyrolysis, and other surface reactions that may take place have been neglected [Eq. (12)]. Ultimately, an energy balance at the surface is performed [Eq. (13)]. This mainly takes into account the heat transfers by convection and diffusion on the gas side, and, on the solid side, the heat transfers by conduction and transport of chemical enthalpy. For simplicity, heat exchanges by radiation have not been considered at first extent. Furthermore, the ablation rate of fuel is described by an Arrhenius law [Eq. (14)]. The convective and diffusive terms in these equations have been expressed through the product of the difference between the temperature / species mass fractions at the flame zone and at the fuel surface, and a convective / diffusive coefficient, respectively. This latter has been computed from the C_f expressions by applying the Reynolds analogy: $\frac{h_D}{h_{conv}} = \frac{D_{diff}}{k} \left(\frac{Sc}{Pr} \right)^{1/3} \approx \frac{1}{\rho c_p}$ and $St = \frac{Nu}{RePr} \approx \frac{C_f}{2}$, where $Nu = \frac{h_{conv} D}{k}$. In this way, for the gaseous convective term in Eq. (13), we have $-k_g \frac{\partial T}{\partial \eta}\Big|_{s^+} = h_{conv}\left(T_s - T_{fl} \right)$. The conductive heat term in Eq. (13) is obtained by the resolution of the transient heat equation for a semi-infinite solid. At the steady-state, this is given by $k_f \frac{\partial T}{\partial \eta}\Big|_{s-} = \rho_f v_r c_{p,f} (T_s - T_{ref})$. More details about this model can be found in Quero Granado et al.[13]

$$\underbrace{\rho_s v_s}_{\text{Mass flux of gases}} = \underbrace{\rho_f v_r}_{\text{Mass flux of fuel by ablation}} \tag{11}$$

DOI: 10.13009/EUCASS2022-5651

Table 1: Thermophysical properties of the HDPE,[19] HTPB[5,19] and PMMA[11,19] solid fuels.

Fuel	**HDPE**	**HTPB**	**PMMA**
Pyrolysis product	C_2H_4	C_4H_6	$C_5H_8O_2$
A_d	4780 m/s	3.965 m/s ($T_s \leq 722$ K) 0.01104 m/s ($T_s > 722$ K)	2.82×10^9 s^{-1}
E_a	125.604×10^3 J/mol	13.35×10^3 cal/mol ($T_s \leq 722$ K) 4.91×10^3 cal/mol ($T_s > 722$ K)	185.8×10^3 J/mol
ρ_f	960	920	1100
$c_{p,f}$	1255.2	1632	1549
k_f	0.1549	0.1506	0.19
ΔH_{pyr}	2.72×10^6	1.8×10^6	9.66×10^5
$\mathcal{M}_k$	0.028	0.054	0.100

$$\underbrace{\rho_{s+} v_{s+} Y_{k+}}_{\text{Mass flux of species } k \text{ by the gaseous flow}} - \underbrace{\rho_{s^+} D_{diff} \left.\frac{\partial Y_k}{\partial \eta}\right|_{s^+}}_{\text{Diffusion mass flux of species } k} = \underbrace{\dot{\omega}_k(T_s)}_{\text{Production mass flux of species } k \text{ by reaction with the fuel surface}} \tag{12}$$

$$\underbrace{\sum_{k=1}^{N_{sp}} \dot{\omega}_i [\Delta H^0_{f,k} + \int_{T_{ref}}^{T_w} c_{p,k}(T)\, dT]}_{\text{Chemical flux from pyrolysis}} - \underbrace{k_g \left.\frac{\partial T}{\partial \eta}\right|_{s+}}_{\text{Convective flux}} = \underbrace{- k_f \left.\frac{\partial T}{\partial \eta}\right|_{s-}}_{\text{Heat flux in fuel}} + \underbrace{\rho_f v_r (\Delta H^0_{f,s} + c_{p,s}(T_s - T_{ref})}_{\text{Enthalpy transport from fuel by regression}} \tag{13}$$

$$v_r = A_d \exp\left(-\frac{E_a}{R T_s}\right) \tag{14}$$

3. Sensitivity Analysis of the 1.5-D combustion Chamber Model

The combustion modeling inside the chamber and the energy balance performed at the fuel surface play a key role in the fuel ablation process, allowing the computation of the fuel regression rate, one of the main outputs employed to characterize HREs and that will permit the later calculation of other engine performances, such as the thrust and the specific impulse. In a HRE, fuel consumption is strongly coupled to the aero-thermo-chemical phenomena of the flow that are influenced at the same time by the numerical parameters entered into our simulation. Here, a sensitivity analysis has been performed with the most important parameters that might have a non-negligible impact on fuel pyrolysis.
The studies have been realized at the steady-state regime, employing a reference case consisting of a cylindrical combustion chamber of $D = 25$ mm and $L = 240$ mm, and a nozzle of $D_{th} = 12.4$ mm and $A_{th}/A_{out} = 6.3$, general dimensions retrieved in the HYCAT engine. Here, it has been decided to perform most of the simulations with a 1-D nozzle model to allow the computations of thrust and specific impulse, which require the knowledge of the throat diameter and the nozzle expansion ratio. The nozzle geometry has remained the same in all the simulations, fixing in this way, the HRE we are testing. Most studies have been performed using O_2 as oxidizer since it is one of the most commonly employed in HREs; and HDPE as fuel, predominantly used in our laboratory tests. Table 1 summarizes the reference thermophysical properties used for the simulations of this fuel, hydroxyl-terminated polybutadiene (HTPB) and polymethyl methacrylate (PMMA).
Three types of parameters have been considered in this analysis. These relate to the aerodynamic variables at the combustion chamber entrance, the thermochemical quantities of the fuel in the GSI model, and the geometric characteristics of the fuel block. In the following subsections the impact of each of the different parameters is presented in terms of the regression rate, the temperature and pressure inside the chamber, the engine thrust or the specific impulse.

3.1 Influence of the Aerodynamic Parameters at the Combustion Chamber Entrance

This study concerns the influence of some parameters related to the aerodynamics of the flow used as inlets to the combustion chamber such as: the oxidizer mass flux, the inlet temperature, the chamber pressure, and the effect of mass fraction of H_2O with respect to H_2O_2 in case of a catalytic injection.

DOI: 10.13009/EUCASS2022-5651

3.1.1 Oxidizer Mass Flux

According to Marxman and Gilbert's limited diffusion theory,[21] the main parameter controlling the regression of fuel is the total mass flux through the channel of the fuel block. This mass flow is fed by the injection of the oxidizer and the addition of mass of fuel resulting from pyrolysis. Because the oxidizer predominates the composition, the total mass flux can be approximated by the oxidizer part [see Eq. (15)].

$$v_r = aG_{tot}^n \approx aG_{ox}^n = a\left(\frac{\dot{m}_{ox}}{\pi r^2}\right)^n \tag{15}$$

In this section, the influence of the oxidizer mass flux, G_{ox}, on the ablation rate has been assessed. Simulations have been performed at different oxidizer mass fluxes and at an inlet temperature, T_{ox}, of 300 K for three different fuels (HTPB, HDPE and PMMA) and gaseous oxygen as oxidizer. Nevertheless, in this subsection, only comments on the influence of G_{ox} are made. The effect of fuel will be addressed in Sec. 3.2.5.
Figure 2(a) represents the fuel regression rate (v_r) dependence with the oxidizer mass flux for the three O/F combinations. A power law of the form of Eq. (15) can be successfully derived ($R^2 \approx 1$) for all of them, being thus in correspondence with Marxman and Gilbert's analysis, meaning an increase of v_r with G_{ox} associated to the enhancement of the heat transfers to the fuel surface. Concerning the axial distribution of the regression rate, this one diminishes along the chamber until a minimum value, from which it starts to grow until the end of the channel [Fig.2(b)]. This shape has already been retrieved in other experimental and numerical studies.[5,7,10]When looking at the local v_r shape non-dimensioned with respect to the maximal value of v_r (usually found at the entrance of the fuel block) we observe that fuel consumption distribution becomes more pronounced for lower oxidizer mass fluxes. This effect is related to the $C_{f0}/C_{f0,D}$ curve, more pronounced and providing larger values for lower Re [see Eq. (10)]. Moreover, when increasing G_{ox}, the mass flow passing through the nozzle increases too, which will produce the growth of the pressure inside the chamber (P_{ch}) that is necessary for a choked flow in the nozzle [Eq. (16)]. Finally, the thrust (F) and specific impulse (I_{sp}) can be deduced from Eqs. (17) and (18), respectively, where a combustion efficiency of $\eta_c = 0.89$ has been taken for all the studies on the basis of the values found in the HYCAT experimental tests. The increase in the computed P_{ch} with G_{ox} generates a similar increase of F too. However, the dependence of I_{sp} with G_{ox} is not the same, tending toward an approximately constant value when boosting G_{ox} [Fig.2(c)]. This is because when increasing G_{ox}, the O/F mass ratio increases, reducing the characteristic velocity (c^*), compensating the growth of the thrust with the mass flux [see Eq. (18)]. The axial velocity component (u_e) rises with G_{ox}, producing a thinner BL and thus, a flame closer to the wall in dimensional terms. In addition, on account of the increase in P_{ch}, the flame temperature (T_{fl}) computed by CEA will increase too, since the O/F ratio employed for its computation is equal to the stoichiometric value and thus, does not change for a given couple [Fig.2(d)].

$$P_{ch} = \frac{\eta_c \dot{m}_{out} c^*}{S_{th}} \tag{16}$$

$$\begin{cases} F = c_F P_{ch} S_{th} \\ c_F = \sqrt{\left(\frac{2\gamma^2}{\gamma-1}\left(\frac{2}{\gamma+1}\right)^{\frac{\gamma+1}{\gamma-1}}\left[1-\left(\frac{P_{out}}{P_{ch}}\right)^{\frac{\gamma-1}{\gamma}}\right]\right)} + \frac{P_{out}-P_{amb}}{P_{ch}}\frac{S_{out}}{S_{th}} \end{cases} \tag{17}$$

$$I_{sp} = \frac{F}{\dot{m}_{out} g} \tag{18}$$

3.1.2 Oxidizer Inlet Temperature

The temperature of the oxidizer injected into the combustion chamber, T_{ox}, influences the combustion process in the channel since its variation implies a change in the flow energy, impacting thus the regression rate values and the engine performances. Here, simulations have been performed for several T_{ox} and three fuels at $G_{ox} = 200$ kg/m^2/s.
From the ideal gas law [Eq. (5)], at a nearly constant pressure, the increase in T_{ox} leads to a decrease in the gas density, and thus, to an increase in the axial velocity for a fixed mass flux. Besides, the flame temperature computed by CEA increases with T_{ox}, and the higher Re and temperatures in the flow lead to an enhancement of the convective heat of the gas transmitted to the wall, increasing thus, the fuel regression and the surface temperature [Fig.3(b)]. Figure 3(a) depicts the dependence of v_r upon T_{ox}. Here, an increase of v_r lower than 9.5% is found for all the fuels studied. Durand[6] found the same influence for v_r and T_s, withal, in his study, the variations on the space-averaged regression rate were between 16 to 19% for a variation of 20% in the inlet temperature reference value, being thus larger than the ones obtained here (of about 0.2 to less than 3.0%). This difference could be due to the consideration of a turbulent fluctuations modeling in Durand's simulations: indeed, the increase in T_{ox} provokes a rise in the kinetic energy level of

DOI: 10.13009/EUCASS2022-5651

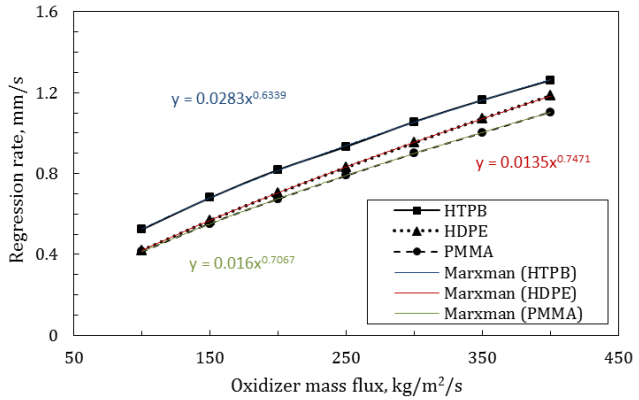

(a) Fuel regression rate dependence on G_{ox} for several fuels with O_2.

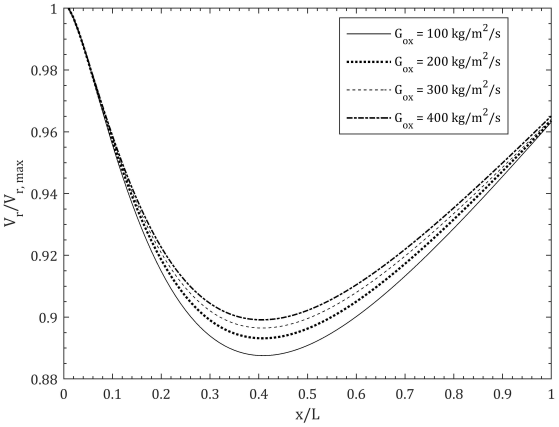

(b) Local fuel regression rate for several G_{ox} (O_2/HDPE).

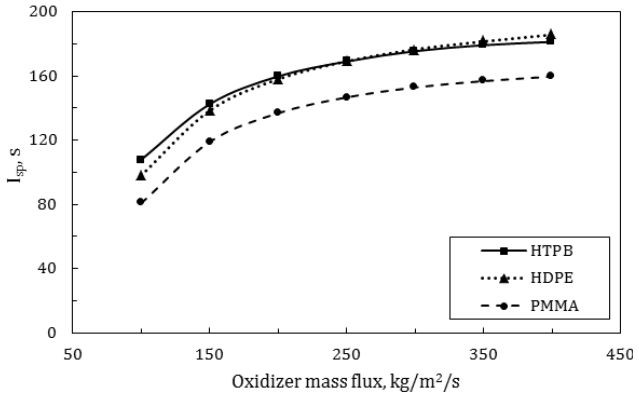

(c) Specific impulse dependence on G_{ox} for several fuels with O_2.

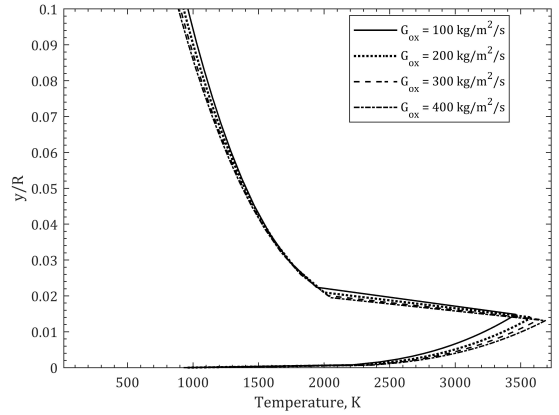

(d) Radial temperature distribution at x/L=0.5 for several G_{ox} (O_2/HDPE).

Figure 2: Influence of the oxidizer mass flux on the HRE performances at T_{ox}=300 K.

the fluctuations in the BL, intensifying in this way the energy transfers to the fuel surface. It has been observed from these graphs that the impact of T_{ox} on the engine performances is more compelling for the lower temperature values though. From T_{ox} =700 K, v_r values remain practically constant since Q_{conv} does not change substantially. Yet, the large amount of fuel mass flux generated by the higher inlet temperatures results in a blowing effect that contributes to diminish the temperature gradient between the flame and the surface, pushing the flame further from this one. This temperature gradient can be diminished in a 23.3% between the 300 K and 700 K inlet temperature cases, preventing a much larger increase in v_r than the one actually obtained. On account of the slight increase in total mass flux with T_{ox}, the P_{ch} imposed by the choked flow in the nozzle, as well as the thrust and the I_{sp} variables, will increase too. All these observations are applied to the three couples studied.

3.1.3 Inlet Combustion Chamber Pressure

Several HRE studies in literature have focused on the evaluation of the pressure influence on the regression rate value. Although some discrepancies exist concerning its precise influence, all of them conclude that pressure does not have a significant impact on regression rate[5,9,24] except when radiation phenomenon is important and the oxidizer mass flux is small (G_{ox}< 150 kg/m^2/s). For this study, simulations have been performed for a combustion chamber only, by imposing the pressure value at the inlet of the numerical domain. Figure 4(a) depicts the evolution with pressure of the ratio of the computed regression rate at a given pressure in comparison to the one obtained at P_{in}=0.5 MPa for several inlet temperatures, showing a growing tendency of v_r (up to 11.6%) with P_{in}. The v_r dependence is essentially greater at lower pressure values and lightly more significant at higher T_{ox}. This analysis has been made also at several oxidizer mass fluxes, showing also a slightly greater impact of v_r for higher G_{ox}. Experimental observations of Favaro et al.[9] and Risha et al.[22] as well as the numerical simulations of Lestrade (1.5-D model)[20] found that the regression rate

DOI: 10.13009/EUCASS2022-5651

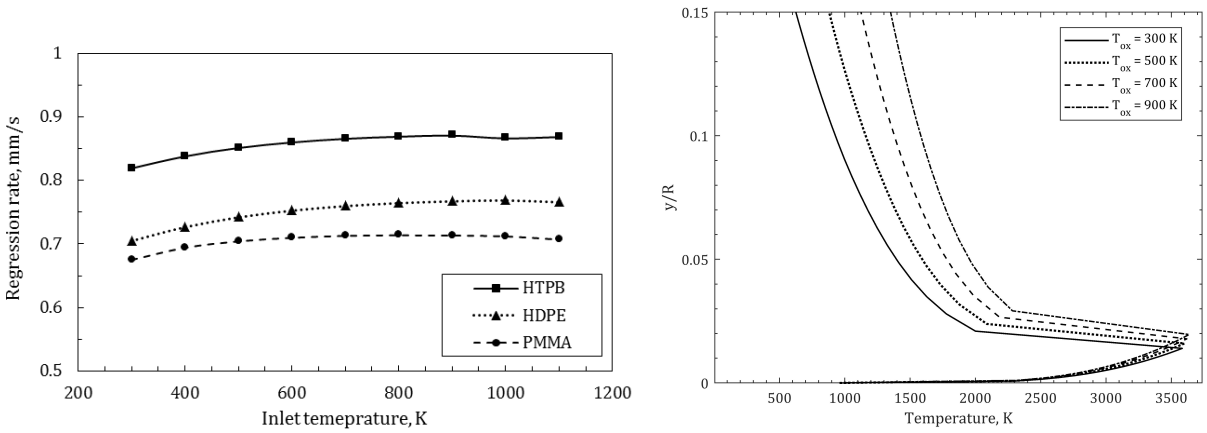

(a) Fuel regression rate dependence on T_{ox} for several fuels with O_2. (b) Radial temperature distribution at x/L=0.5 for several T_{ox} (O_2/HDPE).

Figure 3: Influence of the oxidizer temperature on the HRE performances at G_{ox}=200 kg/m^2/s.

decreased when increasing the chamber pressure, though. Separately, other experiments[14,24] showed a slight increase of v_r with pressure; an effect amplified at lower pressure values and higher mass flow rates, which is in agreement with our findings. The effect on v_r has been also included by some empirical correlations[8,15]through Eq. (15).
The combustion temperature computed by CEA grows with pressure. As a result of the higher flame temperatures obtained [Fig. 4(b)], a larger amount of heat flux will be transferred to the wall, producing thus, higher regression rates and fuel mass fluxes that will slightly increment the distance between the flame and the fuel surface, and diminish the temperature gradient in this zone through the blowing effect. The boost in the pyrolysis production found at higher chamber pressures, generate a larger ethylene mass fraction, and by consequence, smaller H_2O and CO_2 mass fractions at the wall. The high pressure of the gas and the corresponding smaller axial velocity effects for a specific G_{ox} and T_{ox} are compensated, resulting in a BL thickness that barely changes for the different cases simulated.

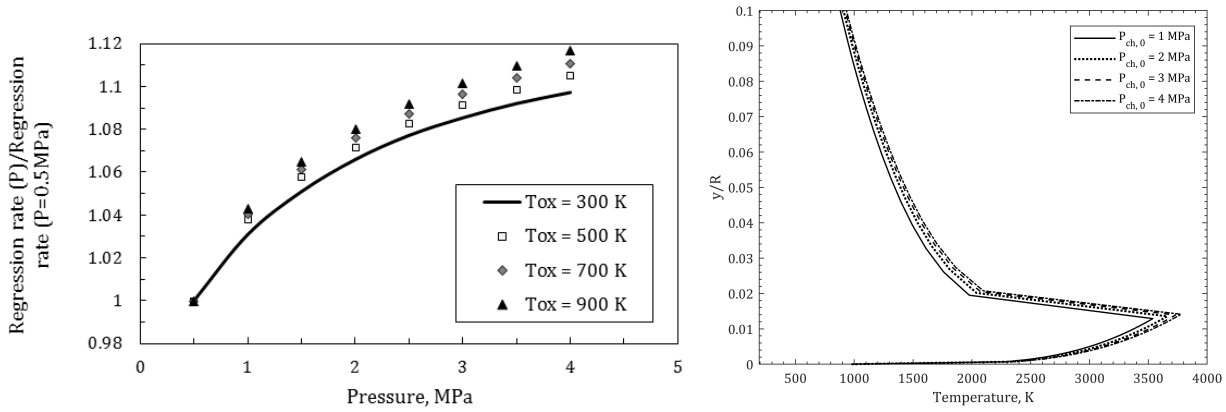

(a) Fuel regression rate dependence on P_{in} for several inlet temperatures. (b) Radial temperature distribution at x/L=0.5 for several P_{in}.

Figure 4: Influence of the inlet pressure on the HRE performances at G_{ox}=300 kg/m^2/s for the O_2/HDPE couple.

3.1.4 Mass Fraction of H_2O in a Catlytic Injection

This analysis focuses on the influence of the proportion of the H_2O species in the H_2O_2 oxidizer during a catalytic injection. Because our HYCAT engine uses this type of injection, it was considered important to perform this study to have an idea of this impact on the engine performances for future experimental tests. In a catalytic injection, the liquid H_2O_2, which can contain H_2O, is decomposed into gaseous dioxygen and water vapor at high temperatures. Hence, the simulations have been performed for a mix of gaseous O_2 with H_2O at T_{ox}=900 K and for several G_{ox} values. Here, Y_{H2O} corresponds to the mass fraction of the H_2O species with respect to H_2O_2, and has been varied from 0 to 0.3.

DOI: 10.13009/EUCASS2022-5651

Table 2: Relative differences in the pyrolysis enthalpy of HDPE fuel and their impact on the computed variables.

$\varepsilon(\Delta H_{pyr})$, %	$\varepsilon(v_r)$, %	$\varepsilon(T_s)$, %	$\varepsilon(P_{ch})$, %	$\varepsilon(F)$, %	$\varepsilon(I_{sp})$, %	$\varepsilon(\dot{Q}_{conv})$, %
-20.0	10.74	0.65	3.40	5.36	4.07	-5.99
+20.0	-8.65	-0.57	-2.88	-4.51	-3.55	5.18

We have observed that as Y_{H2O} increases, fuel regression rate diminishes. This reduction is slightly more consequent for higher G_{ox}, and can go to 17% when Y_{H2O}=0.3, being thus non-negligible. The diminution of total mass flux with the H_2O species will impose smaller pressures in the chamber (decreased by 7% at most for the range of the parameters studied) that will induce at the same time a lesser thrust (up to 18.4% diminution) and I_{sp} value (16.8% reduction) since, in Eq. (18), the impact of Y_{H2O} on F is larger than the one made to $\dot{m}_{out}$ for a specific G_{ox}. These reductions will be more important for lower G_{ox}, contrarily to what happens with v_r. The flame temperature weakens when Y_{H2O} is increased [see Fig.5(a)]. This, by consequence, will reduce the convective heat transfer to the wall and the temperature gradient in the BL, thus, decreasing the fuel consumption and the surface temperature. However, the presence of H_2O will be more important throughout the BL and at the fuel surface [Fig.5(b)], which, together with the reduction of pyrolysis production at higher Y_{H2O}, will generate a diminution in the fuel mass fraction.
Kang et al.[17] found higher increments in v_r while increasing the concentration of H_2O_2 from 90 to 95% (around 28.1%). This trend is in agreement with our findings, withal the relative growth of our v_r for these Y_{H2O} was of 2.3%.

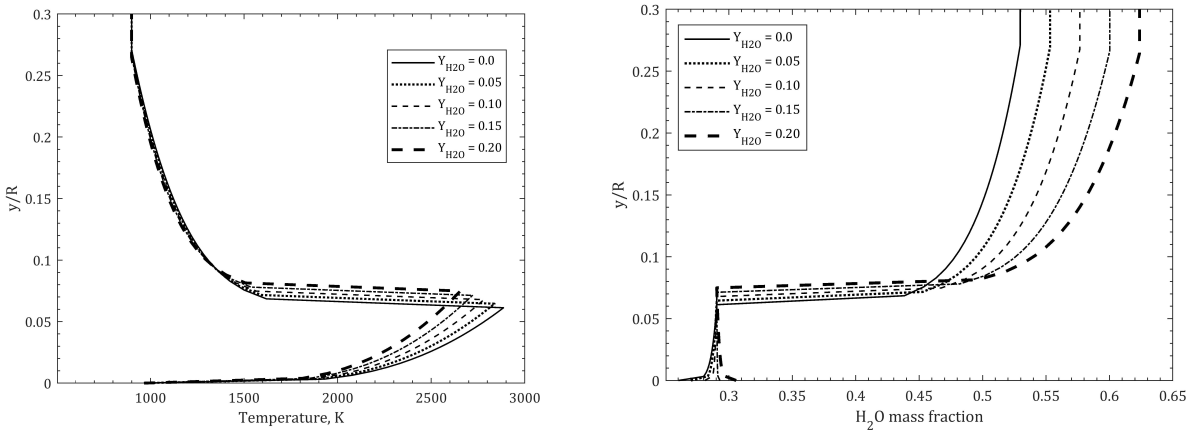

(a) Radial temperature distribution at x/L=0.5 for several inlet Y_{H2O}. (b) Radial H_2O mass fraction distribution at x/L=0.5 for several inlet Y_{H2O}.

Figure 5: Influence of Y_{H2O} in H_2O_2 oxidizer with HDPE on the HRE performances at G_{ox}=300 kg/m^2/s and T_{ox}=900K.

3.2 Thermochemical Parameters

In the present section, the thermo-chemical parameters intervening in the energy balance equation at the solid / gas interface of the GSI model presented in Sec.2 will be assessed in order to define their influence on the HRE performances. These are conformed by: the enthalpy of depolymerization of the material; the two Arrhenius coefficients appearing in the pyrolysis law; the density and specific heat of the solid; the fuel employed; and finally, although not constituting a fuel property, the addition of a radiative heat source to the total heat transmitted to the fuel surface.

3.2.1 Enthalpy of Pyrolysis

The enthalpy of pyrolysis (ΔH_{pyr}) is a property of the fuel that depends on the material composition, the manufacturing process, the use of additives, etc. The influence of this parameter on the regression rate must thus be characterized. Simulations have been carried out for relative differences (ε) of ±20% in ΔH_{pyr} with respect to the reference value of 2.72×10^6 J/mol.[19] Table 2 shows the retrieved relative discrepancies of the variables of interest for both cases.
The decrease of ΔH_{pyr} in a 20% generates the increase of v_r due to the lower necessary energy to pyrolyze the fuel. The more important v_r will lead also to an increase of the surface temperature through the Arrhenius law. Additionally, the larger amount of mass passing through the nozzle produces a rise in the required chamber pressure that, at the same time, leads to the increase in thrust and I_{sp} for a given G_{ox}. The slight change in pressure does not produce a significant

DOI: 10.13009/EUCASS2022-5651

Table 3: Relative differences in the pre-exponential Arrhenius coefficient and their impact on the computed variables.

$\varepsilon(A_d)$, %	$\varepsilon(v_r)$, %	$\varepsilon(T_s)$, %	$\varepsilon(P_{ch})$, %	$\varepsilon(F)$ %	$\varepsilon(I_{sp})$, %	$\varepsilon(\dot{Q}_{conv})$, %
-20.0	-0.60	1.40	-0.14	-0.23	-0.16	-0.13
+20.0	0.48	-1.12	0.18	0.27	0.22	0.10

Table 4: Relative differences in the activation energy of HDPE and their impact on the computed variables.

$\varepsilon(E_a)$, %	$\varepsilon(v_r)$, %	$\varepsilon(T_s)$, %	$\varepsilon(P_{ch})$, %	$\varepsilon(F)$, %	$\varepsilon(I_{sp})$, %	$\varepsilon(\dot{Q}_{conv})$, %
-20.0	8.70	-19.57	2.89	4.56	3.52	1.47
+20.0	-8.01	19.37	-2.60	4.07	3.18	-1.95

change in T_{fl} though, and the larger amount of fuel mass injected at higher temperatures diminishes the temperature gradient in this region and increases the distance between the reaction zone and the wall. The higher pressures in the chamber lead to smaller axial velocities. Finally, the larger flux of pyrolyzed fuel from the surface as well as the lower diffusion coefficient (h_D) associated to the smaller Re, engender a raise of the fuel mass fraction at the surface.
The most affected variable by ΔH_{pyr} has been the fuel regression rate, with variations of around 10%. The fuel surface temperature is hardly modified and the deviations of the other variables are not very significant (around 5%). These observations corroborate the trends of Bianchi et al.,[3] who observed a 20.9% increase in the fuel regression rate for a 30% decrease in the enthalpy of pyrolyzation. Our results are also in agreement with those of Durand's,[6] who found a closer influence of ΔH_{pyr} on v_r (3.8% increase by a 4.5% underestimation of ΔH_{pyr}).

3.2.2 Arrhenius Coefficients of the Regression Rate Law

This analysis concerns the coefficients intervening in the Arrhenius law [Eq. (14)] that describes the regression rate of the solid combustible in our 1.5-D model: the pre-exponential coefficient A_d, and the activation energy of the fuel E_a. This latter relies upon the chemical transformation that takes place during pyrolysis and the nature of the reacting species. Their values depend thus on the pyrolyzed fuel and may vary from one reference to another. Therefore, two separate studies about the impact of these coefficients on the HRE performances have been tackled in this paper.

Pre-exponential Coefficient, A_d

This study has been made by determining the influence on the results when inflicting a 20% variation on A_d with respect to the reference value, taken as 4780 m/s for the HDPE fuel.[19]
From Table 3, it is observed that variations in this parameter hardly affect the variables of interest. Indeed, a 20% decrease of this coefficient generates a reduction in the regression rate value of 0.6% only. Hence, v_r seems insensitive to A_d and, by consequence, total mass fluxes are not barely modified by this parameter. The corresponding reduction in the chamber pressure is not substantial either, and thus, nor are the ones of the engine thrust or the I_{sp}. The structure of the turbulent BL is practically unaffected too. Hence, it is possible to observe easily through the Arrhenius law [Eq. (14)] that only T_s will be mostly altered, and that a reduction of A_d will imply a lightly boost in the wall temperature. Indeed, the variations of this variable are greater than those obtained by ΔH_{pyr} variation (1.12 to 1.40%). This trend coincides with that of Durand,[6] who observed that a 20% decrease in A_d with respect to their reference value led to an increase of about 12.2 K over the fuel surface temperature, whereas in our case this is about 13.45 K. Bianchi et al.[3] also remarked a growth in T_s from 30 to 40 K and a 1.6% drop of v_r due to a 44% decrease of the pre-exponential coefficient, which is also in agreement with our results.

Activation Energy, E_a

Here, the impact of the variations of 20% in this parameter with respect to the reference value of 125.604 kJ/mol[19] have been assessed. The activation energy is the necessary energy for a reaction to occur and defines the rate of this one. A decrease in E_a induces a more rapid initiation of the reaction, increasing thus, the regression rate of the solid and the received convective heat. In contrast, the wall temperature follows the opposite trend to v_r, with differences that are close to the corresponding variations of E_a (around 19.4%). The Arrhenius law [Eq. (14)] highlights the proportional relationship between these two by considering a reasonable change in the fuel mass flow. Moreover, because the mass flux is higher, the pressure in the chamber and thrust are too, and I_{sp} will grow since the retrieved change in $\dot{m}_{out}$ is not as remarkable as for F in Eq. (18). The increase in fuel production also contributes to increment the mass fraction of ethylene at the surface. Table 4 shows the influence of the variations in E_a on several important computed variables.
In comparison to bibliography, Durand[6] found an increase / decrease of 22.8% / 17.7% in v_r for an underestimation / overestimation of 20% of E_a with respect to the reference value, as well as a decrease / increase of 180 K (18.9%)

DOI: 10.13009/EUCASS2022-5651

/ 170 K (18.3%) in T_s for the same amount of variation. These T_s values are similar to those found in our analysis. However, the effect predicted by our code on v_r is much less important than the one found by Durand. Yet, Bianchi et al.[3] obtained a 33% increase in T_s for an elevation of the activation energy of 39%, while the impact on v_r resulted in a decrease of 11.6% only, being hence, more in agreement with our results.

3.2.3 Fuel Density

The fuel density (ρ_f) constitutes a physical property of the solid stored in the combustion chamber. It is involved in the calculation of the mass flux of burnt fuel during the pyrolysis process. A sensitivity study has been carried out to determine the impact of this parameter on the variables of interest of a HRE. For this purpose, the fuel density has been varied between 910 and 980 kg/m^2/s, interval that corresponds to the range of values between which a PE type of fuel (including LDPE and HDPE) can vary. Simulations have been made for T_{ox}=300 K and G_{ox}=200 kg/m^2/s.
For a given amount of transmitted heat to the surface, the increase in ρ_f results in a diminution of the fuel regression rate at a given ΔH_{pyr} and thus, a slight decrease in T_s. However, the decrease in v_r is slower than the increase in ρ_f, resulting in a general slight increase of the fuel mass flux. Consequently, this leads to a pressure in the chamber that is slightly higher, which will also contribute to increment the thrust and I_{sp} values. The BL structure and the combustion temperature are scarcely affected though. The corresponding differences of these variables turn out to be smaller than 0.10%, and thus, negligible. Only the fuel regression rate is sensitive to this parameter. Indeed, the variation of ρ_f in the defined range of values (equivalent to a 7.14% variation), produces a 7.48% variation in v_r, being both of them approximately of the same amount. Therefore, the influence of fuel density on v_r can be considered to be somewhat of importance despite the fact that the corresponding relative changes are not very high in absolute value.

3.2.4 Specific Heat Capacity of Fuel

The fuel specific heat capacity ($c_{p,f}$) is a physical property of the material that intervenes directly in the computation of the conductive heat flux, playing thus a role in the energy balance and heat transmission to the surface, and influencing the fuel pyrolysis process. The range of this parameter in this sensitivity analysis has been quite wide, going from 1250 J/kg/K to 2600 J/kg/K, covering the literature data values for PE, LDPE and HDPE fuels.[11,19]This range represents a maximal variation of around 50%. Simulations have been made for T_{ox}=300 K and G_{ox}=200 kg/m^2/s.
The increase of $c_{p,f}$ brings along the increase of the amount of heat that must be added to the material to generate a rise in temperature. Assuming that the added heat to the fuel remains approximately constant, this will mean a decrease in the surface temperature of fuel, being in this way, closer to the established T_{ref} of the material (300 K). The decrease of T_s will induce through the Arrhenius law a smaller v_r. The flux of conductive heat delivered to the gas will acquire a bigger importance with respect to the heat flux of depolymerization when compared to the reference case. Additionally, chamber pressure, combustion temperature, thrust and I_{sp} are reduced. Moreover, because of the diminished pyrolysis production at the solid surface, the mass fraction of fuel becomes also smaller. The variation of $c_{p,f}$ in the studied range may produce changes of a similar amount in Q_{cond} (43.88%) and a maximal variation of 15.22% in v_r for the simulated conditions. The resulting largest modifications found in averaged chamber pressure (4.62%), engine thrust (7.39%) and specific impulse (5.76%) are more attenuated though, and the impact on T_s is negligible (0.90%).

3.2.5 Type of Fuel

The analysis performed in this section focuses on the influence that the solid fuel stored in the combustion chamber has on the computed results for several G_{ox} and T_{ox} values. In particular, HTPB, HDPE and PMMA fuels are studied with O_2 as oxidizer. The figures presented in Secs. 3.1.1 and 3.1.2 are employed to perform the study.
From Fig.2(a) and Fig.3(a) we observe that HTPB fuel provides larger regression rates than the other two in all the cases, and that the ablation rates of HDPE and PMMA are very similar. This is in correspondence with the empirical correlations from literature.[16,28] The temperature resulting from the combustion process differs only around 40 K from each fuel. However, in view of the solid and gaseous fuel thermophysical properties, temperature at the surface for PMMA is larger than for the other two and the flame is situated closer to the wall [see Fig.6(a)]. However, the lower E_a values for the HTPB and HDPE fuels with respect to PMMA compensate the effect of a higher surface temperature, providing consequently v_r values that are larger for the former two, especially for HTPB [see Eq. (14)]. Because of the fuel density values, the largest fuel mass fluxes are found for HTPB at lower G_{ox} and for PMMA at $G_{ox} > 200$ kg/m^2/s. Nevertheless, the higher characteristic velocities (c^*) of HDPE and HTPB with respect to PMMA, compensate the effect of the smaller fuel mass fluxes and $\dot{m}_{out}$ in Eq. (16), leading to P_{ch}, thrust and I_{sp} values that are similar and more important for the HTPB and HDPE fuels than for PMMA [Fig.2(c)]. Concerning the influence of T_{ox} on v_r, this one is more significant for the HDPE fuel (9% growth from 300 K to 1000 K) than for HTPB (6%) and PMMA (5.5%).

DOI: 10.13009/EUCASS2022-5651

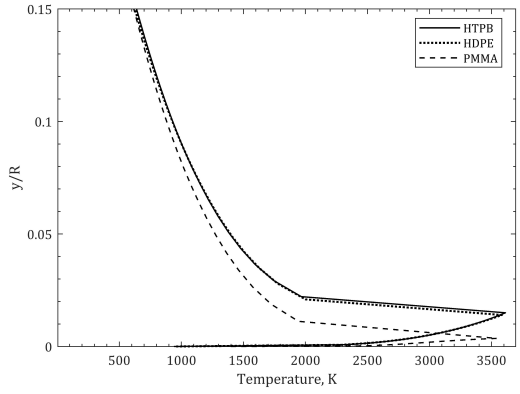

(a) Radial temperature distribution at x/L=0.5 for several fuels with O_2 and G_{ox}=200 kg/m^2/s.

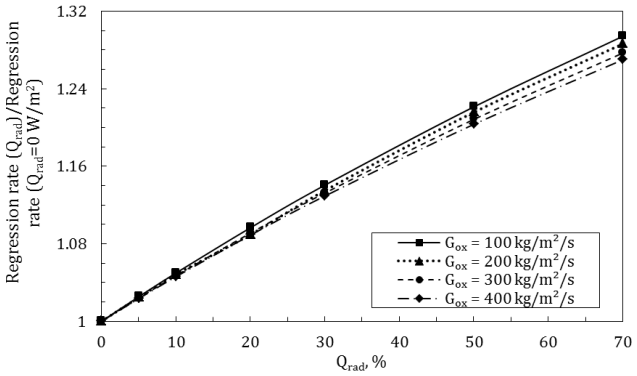

(b) Dependence of the ratio of fuel regression rates with and without a radiative heat flux source contribution (O_2/HTPB).

Figure 6: Influence of the thermomechanical parameters on the HRE performances at T_{ox}=300 K.

3.2.6 Radiative Heat Flux

Radiative heat fluxes have been neglected during the formulation of this model. However, in certain situations, they may acquire a major importance over the turbulent convective heat transfers, producing an increase of 1 to 35% in the obtained fuel regression rate.[3,5,21] Fuels such as HTPB are exposed to significant radiative heat at low mass fluxes or fuel rich mixtures due to an important production of soot particles that can account up to 80% of the total radiative flux[5] while the rest of radiation is due to the gas. Empirical expressions quantifying soot radiation only exist for the O_2/HTPB couple.[25] However, a general combustion chamber model, applicable to all sorts of O/F couples, is searched. Hence, a study about the influence of a supplementary thermal flux source that would act as a radiative one has been performed for the O_2/HTPB couple. The "radiative" heat has been quantified by defining a percentage of the convective heat flux value (from 0% to 70% of Q_{conv}) that would be added to the heat transmitted to the fuel surface. Simulations have been performed for a combustion chamber only, T_{ox}=300 K, P_{in}=2.4 MPa, and several oxidizer mass fluxes.
The imposed heat flux source contributes to increase the total heat transferred to the wall, generating an approximately linear rise of the fuel surface temperature and ablation rate (to around 30%) that is more important for the lower G_{ox} values [Fig.6(b)], which is in agreement with the references. Flame temperature has not barely changed with Q_{rad}, since neither the fuel, T_{ox} nor P_{ch} change either. As a consequence of a higher T_s when Q_{rad} increases, the temperature difference between the flame and the wall diminishes, and thus, Q_{conv} diminishes too, preventing a more important increase of v_r. Furthermore, the larger mass of burnt fuel generates an increase of the fuel mass fraction at the surface.

3.3 Influence of the Geometrical Parameters

In this section, the impact of parameters affecting the geometrical characteristics of a cylindrical combustion chamber has been analyzed, in particular, the chamber size and the number of channels constituting the fuel block.

3.3.1 Block Diameter

Scale-up effects on fuel regression rate have already been studied by several researchers before.[4,8]These effects are considered of great importance for the development of larger size motors when extrapolating sub-scale experimental data for their design, since it can lead to large errors. Simulations have been made for the combustion chamber only to avoid including an important pressure effect on the results that would be associated to the big total mass flow differences through the nozzle between the three engines. The influence of port size was tested for several G_{ox} and three constant diameters (25, 50, 100 mm) at T_{ox}=300 K and P_{in}=2.4 MPa. These diameters corresponded also to the ones used in Cai et al.'s work.[4] For all the configurations L/D was held constant, with the smallest size being of L=240 m.
Figure 7(a) shows that fuel regression rate decreases when increasing the port diameter for a specific G_{ox}. In particular, v_r diminishes in average 16.6% for D=50 m and around 29.4% for D=100 mm. The scale-up effect has a lesser impact when the oxidizer mass flux increases, confirming the preponderant influence of the latter due to heat of convection. Cai et al.[4] found similar v_r losses, being around 13.6% for D=50 mm and 28.2% for D=100 mm. For the same G_{ox}, when increasing the port diameter, the flame moves further from the fuel surface, therefore reducing the temperature gradient and the convective heat transfer to the wall. For larger motors, the BL is thicker, withal it occupies a smaller part of

DOI: 10.13009/EUCASS2022-5651

the channel when compared to the port radius. Likewise, the flame is observed closer to the wall in non-dimensional terms, although it is actually further from it. This fact was also observed by Venkateswaran and Merkle.[27]
Moreover, Cai et al. showed by manipulation of Marxman's diffusion theory expressions that the semiempirical formula of Eq. (15) could be expressed in function of the fuel port diameter as: $aG_{ox}^{n}D^{-0.2}$. By representing $v_r D^{0.2}$ in function of G_{ox} for the three sizes [Fig.7(b)], we obtain curves very near to one another, which pretty much agrees with the overlapping that should have been retrieved according to their theoretical findings.

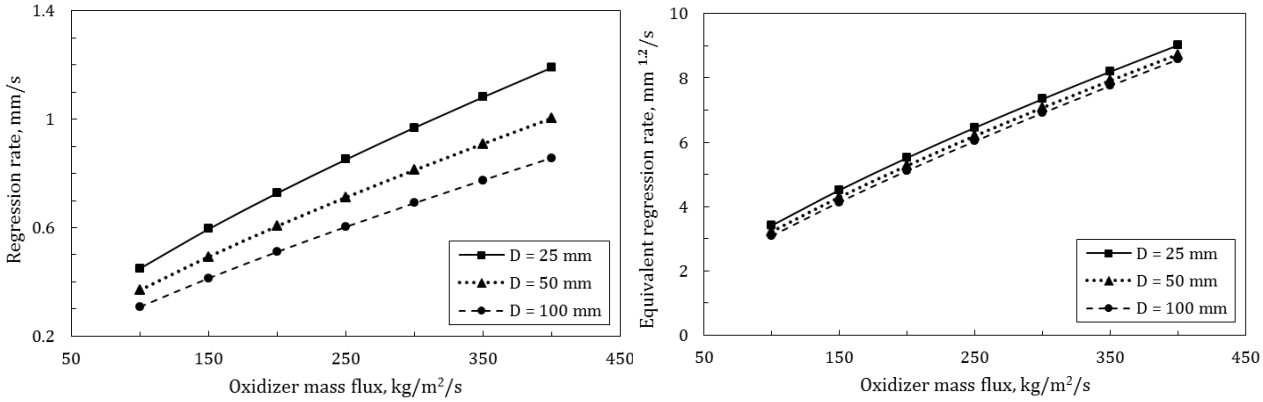

(a) Regression rate dependence on port size for several G_{ox}.

(b) Equivalent regression rate dependence on port size for several G_{ox}.

Figure 7: Scale-up effects on the HRE performances at T_{ox}=300 K for the O_2/HDPE couple.

3.3.2 Multiple Fuel Ports

The low regression rates of HREs are a critical disadvantage that can act as a deterrent to some of their envisionned applications. One method to enhance fuel ablation is to increase the contact area of burning, thus increasing the heat transfer to the wall. This can be achieved by a different design of the interior of the combustion chamber. Several configurations can be contemplated: cylindrical multi-ports, wagon wheel, double D, etc. The impact of a multi-port configuration has been studied in this section due to the capacity of our model to simulate and reproduce the geometry and the involved physics in one of the ports, and extrapolate the solution to the other ports of the block. A uniform consumption across the ports has been considered without analyzing the possible existing interactions between them.
Simulations have been made at T_{ox}=300 K and several oxidizer mass flows ($\dot{m}_{ox,total}$) for blocks with one, two and three ports of same inner diameter. The mass flow injected through each channel is given by $\dot{m}_{ox,j} = \dot{m}_{ox,total}/N$, with N the number of ports. Therefore, the higher N, the smaller the mass flux injected through each channel, which, as seen in Sec.3.1.1, will mean less heat transfers to the fuel and thus, lesser regression rates in every port. Despite this, because the total consumed fuel surface is larger when N>1, the overall fuel mass flow is larger, and more mass is introduced to the nozzle for a given $\dot{m}_{ox,total}$, increasing thus, the chamber pressure, the thrust and the I_{sp}. This latter happening because the increase produced in $\dot{m}_{out}$ is not as pronounced as for F [Eq. (18)]. A smaller O/F mass ratio is also found while increasing N. Figure 8(a) represents the dependence of thrust upon $\dot{m}_{ox,total}$ for the three cases, showing a growth between 3.6% and 20.5% for a three port-configuration with respect to a single-port. When looking at the rate of total ablated thickness [Fig.8(b)], it is observed that the larger the number of ports, the higher this overall rate will be for a specific $\dot{m}_{ox,total}$. In particular, v_r is enhanced between 20.1 and 23.7% when two ports are employed, whilst the enlargement is about 34.4 to 40.9% with three ports. Kim et al.[18] also found higher experimental overall regression rates when increasing the number of ports with the same diameter, although not at the same extent than in our model. For G_{ox}=200-400 kg/m^2/s, they obtained an increase of 24 to 37% for two ports and of 41 to 54% for three ports.

4. Conclusion

The sensitivity analyses performed in this paper concerning the 1.5-D combustion chamber model of a HRE have allowed to determine the parameters introduced in the numerical domain that are more susceptible to have a significant or non-negligible impact on engine performances (fuel regression rate, pressure in the chamber, engine thrust, specific impulse, etc.). These parameters have been classified in three categories in function of the physical effect to which they are related: aerodynamics of the flow, thermophysics of the fuel, and the geometry of the combustion chamber. The influence of these parameters on the performances can be explained by the physics used in the modeling. The retrieved dependence is in agreement with the bibliographic data despite not being of the same intensity for all the

DOI: 10.13009/EUCASS2022-5651

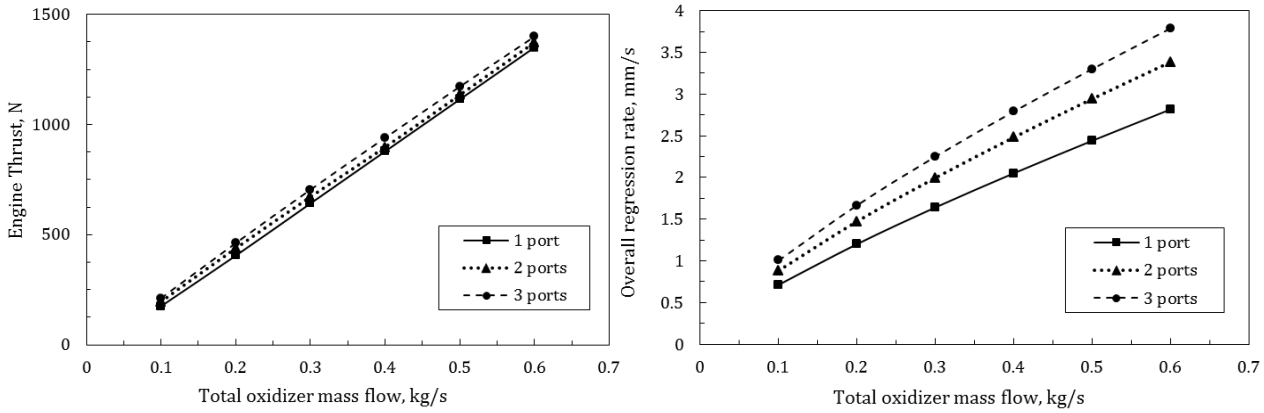

(a) Thrust dependence on port-number and oxidizer mass flow. (b) Regression rate dependence on port-number and oxidizer mass flow.

Figure 8: Impact of the port-number of a fuel block on the HRE performances at T_{ox}=300 K for the O_2/HDPE couple.

cases. The parameters producing the most of the impact on HRE performances have been: the oxidizer mass flux injected to the combustion chamber (increase of 180% of the regression rate while increasing G_{ox} from 100 to 400 kg/m^2/s); the geometric effects such as the motor size (29.4% decay in v_r when passing from a 25 mm diameter to another one of 100 mm) and the presence of multiple ports (generating up to a 40% higher v_r when passing from one to three ports for a given $\dot{m}_{ox}$); and finally, the variables intervening directly on the energy balance at the fuel surface, such as the radiative heat source (28.1% increase in v_r when Q_{rad}=70%Q_{conv}) or the type of solid fuel (21.1% higher v_r for HTPB with respect to PMMA). Finally, our 1.5-D combustion chamber model has been able to correctly simulate the influence of the main parameters involved in the physics of a HRE, which, taking into account the firsts bibliography and experimental verifications performed in previous work, allow to complete the main validation phase of the model.

5. Acknowledgments

Special thanks to ONERA and CNES for financially supporting this research and the Propulsion Laboratory Research Unit of ONERA for the realization of the experimental campaign on the HYCAT test bench.

References

[1] F. Barato, M. Lazzarin, N. Bellomo, M. Faenza, A. Bettella, and D. Pavarin. A numerical model to analyze transient behavior and instabilities on hybrid rocket motors. In *47th AIAA/ASME/SAE/ASEE Joint Propulsion Conference & Exhibit*. AIAA Paper 2011-5538, July 2011.

[2] C. Bayeux, E. Radenac, and P. Villedieu. Theory and validation of a 2D finite-volume integral boundary-layer method for icing applications. *AIAA Journal*, 57(3):1092–1112, March 2019.

[3] D. Bianchi, G. Leccese, F. Nasuti, M. Onofri, and C. Carmicino. Modeling of high density polyethylene regression rate in the simulation of hybrid rocket flowfields. *Aerospace*, 6(88), 2019.

[4] G. Cai, P. Zeng, X. Li, H. Tian, and N. Yu. Scale effect of fuel regression rate in hybrid rocket motor. *Aerospace Science and Technology*, 24(1):141–146, 2013.

[5] M. Chiaverini, G. Harting, K. K. Kuo, and A. Peretz. Regression rate and heat transfer correlations for hybrid rocket combustion. *Journal of Propulsion and Power*, 17(1):99–110, 2001.

[6] J. E. Durand. *Development and Experimental Validation of a Numerical Modeling for the Simulation of a Hyrbid Rocket – Développement et Validation Expérimentale d'une Modélisation Numérique pour la Simulation d'un Moteur Hybride*. PhD thesis, Institut Supérieur de l'Aéronautique et de l'Espace (ISAE), 2019.

[7] J. E. Durand, F. Raynaud, J. Y. Lestrade, and J. Anthoine. Turbulence modeling effects on fuel regression rate in hybrid rocket numerical simulations. *Journal of Propulsion and Power*, 35(6):1–16, 2019.

[8] P. Estey, D. Altman, and J. McFarlane. An evaluation of scaling effects for hybrid rocket motors. In *27th Joint Propulsion Conference*. AIAA Paper 1991-2517, June 1991.

DOI: 10.13009/EUCASS2022-5651

[9] F. Favarò, M. Manzoni, A. Coronetti, L. DeLuca, and S. William. Solid fuel regression rate modeling for hybrid rockets. *Journal of Propulsion and Power*, 29(1):205–215, 2013.

[10] G. Gariani, F. Maggi, and L. Galfetti. Numerical simulation of HTPB combustion in a 2D hybrid slab combustor. *Acta Astronautica*, 69:289–296, Sept. 2011.

[11] N. Gascoin, P. Gillard, A. Mangeot, and A. Navarro-Rodriguez. Literature survey for a first choice of a fuel-oxidiser couple for hybrid propulsion based on kinetic justifications. *Journal of Analytical and Applied Pyrolysis*, 94:1–9, March 2012.

[12] M. Gieras and A. Gorgeri. Numerical modelling of the hybrid rocket engine performance. *Propulsion and Power Research*, 10(1):15–22, 2021.

[13] E. Quero Granado, J. Hijlkema, J.Y. Lestrade, and J. Anthoine. Pseudo-2-dimensional modeling and validation of a hybrid rocket combustion chamber. *Journal of Propulsion and Power*, pages 1–16, June 2022.

[14] D. Helman, M. Wolfshtein, and Y. Manheimer-Timnat. Theoretical investigation of hybrid rocket combustion by numerical methods. *Journal of Combustion and Flame*, 22(2):171–190, 1974.

[15] S. Ito, L. Kamps, and H. Nagata. Fuel regression characteristics in hybrid rockets using nitrous oxide/high-density polyethylene. *Journal of Propulsion and Power*, 37(2):342–348, March 2021.

[16] E. Jens, B. Cantwell, and G. Hubbard. Hybrid rocket propulsion systems for outer planet exploration missions. *Acta Astronautica*, 128:119–130, June 2016.

[17] S. Kang, D. Lee, E. Lee, and S. Kwon. Design and performance evaluation of hybrid rocket using 95 wt.% h2o2. In *52nd AIAA/SAE/ASEE Joint Propulsion Conference*. AIAA Paper 2016-4864, July 2016.

[18] S. Kim, J. Lee, H. Moon, J. Kim, H. Sung, and O.C. Kwon. Regression characteristics of the cylindrical multiport grain in hybrid rockets. *Journal of Propulsion and Power*, 29(3):573–581, 2013.

[19] G. Lengellé, B. Fourest, J. Godon, and C. Guin. Condensed-phase behavior and ablation rate of fuels for hybrid propulsion. In *29th Joint Propulsion Conference and Exhibit*. AIAA Paper 93-2413, June 1993.

[20] J. Y. Lestrade. *Modeling of the Regression of Liquefiable Fuels in a Hybrid Rocket – Modélisation de la Régression des Combustibles Liquéfiables dans un Moteur Hybride*. PhD thesis, Institut Supérieur de l'Aéronautique et de l'Espace (ISAE), 2012.

[21] G. A. Marxman and M. Gilbert. Turbulent boundary layer combustion in the hybrid rocket. *Symposium (International) on Combustion*, 9(1):371–383, 1963.

[22] G. Risha, G. Harting, K. Kuo, A. Peretz, D. Koch, H. Jones, and J. Arves. Pyrolysis and combustion of solid fuels in various oxidizing environments. In *34th AIAA/ASME/SAE/ASEE Joint Propulsion Conference and Exhibit*. AIAA Paper 1998-3184, July 1998.

[23] W. M. Rohsenow, J. P. Hartnett, and Y. I. Cho. *Handbook of Heat Transfer*. McGraw-Hill handbooks. McGraw-Hill Education, New York, 3 edition, 1998.

[24] L. D. Smoot and C. F. Price. Pressure dependence of hybrid fuel regression rates. *AIAA Journal*, 5(1):102–106, 1967.

[25] L. Strand, M. Jones, R. Ray, and N. Cohen. Characterization of hybrid rocket internal heat flux and HTPB fuel pyrolysis. In *30th Joint Propulsion Conference & Exhibit*. AIAA Paper 1994-2876, June 1994.

[26] H. Tian, X. Meng, H. Zhu, C. Li, R. Yu, Y. Zhang, and G. Cai. Dynamic characteristics study of regression rate in variable thrust hybrid rocket motor. *Acta Astronautica*, 193:221–229, Apr. 2022.

[27] S. Venkateswaran and C.L. Merkle. Size scale-up in hybrid rocket motors. In *34th Aerospace Sciences Meeting & Exhibit*. AIAA Paper 1996-647, Jan. 1996.

[28] G. Zilliac and A. Karabeyoglu. Hybrid rocket fuel regression rate data and modeling. In *42nd AIAA/ASME/SAE/ASEE Joint Propulsion Conference & Exhibit*. AIAA Paper 2006-4504, July 2006.

[29] P.M. Zolla, M.T. Migliorino, D. Bianchi, F. Nasuti, R.C. Pellegrini, and E. Cavallini. A computational tool for the design of hybrid rockets. *Aerotecnica Missili & Spazio*, 100(4):387–397, 2021.